

## Article

# Preparation of Fe<sub>3</sub>O<sub>4</sub>/α-MnO<sub>2</sub> Magnetic Nanocomposites for Degradation of 2,4-DCP through Persulfate Activation

Yan Zhao <sup>1,2</sup>, Fei Luo <sup>1</sup> and Rui Zhou <sup>2,\*</sup><sup>1</sup> Shenzhen Academy of Environmental Sciences, Shenzhen 518001, China<sup>2</sup> National Joint Engineering Laboratory for Petrochemical Pollution Site Control and Restoration Technology, Jilin University, Changchun 130021, China

\* Correspondence: zhour@jlu.edu.cn

**Abstract:** In this study, Fe<sub>3</sub>O<sub>4</sub> magnetic nanoparticles (MNPs) were loaded on α-MnO<sub>2</sub> nanowires using an improved hydrothermal synthesis method combined with an ultrasonic coprecipitation method, the loading ratio was optimized, the efficiency of the prepared Fe<sub>3</sub>O<sub>4</sub>/α-MnO<sub>2</sub>-activated persulfate (PS) system for the degradation of 2,4-dichlorophenol (2,4-DCP) was investigated, and the effects of PS concentration, Fe<sub>3</sub>O<sub>4</sub>/α-MnO<sub>2</sub> magnetic nanocomposites (MNCs) dosage, pH value and initial pollutant concentration on the degradation of 2,4-DCP were investigated. The results showed that when the initial concentrations of 2,4-DCP, PS, and Fe<sub>3</sub>O<sub>4</sub>/α-MnO<sub>2</sub> MNCs were 100 mg/L, 30 mmol/L, and 0.4 g/L, the degradation rate of 2,4-DCP reached 96.3% after 180 min of reaction at 30 °C under a neutral condition, and the fitting results showed that the degradation of 2,4-DCP by the Fe<sub>3</sub>O<sub>4</sub>/α-MnO<sub>2</sub>-activated PS system conformed to quasi-first-order kinetics. The degradation of 2,4-DCP by different Fe<sub>3</sub>O<sub>4</sub>/α-MnO<sub>2</sub>-activated PS systems was compared, and a possible PS activation mechanism was proposed. The Fe<sub>3</sub>O<sub>4</sub>/α-MnO<sub>2</sub> MNCs exhibited excellent reusability, and by introducing Fe<sub>3</sub>O<sub>4</sub>/α-MnO<sub>2</sub> MNCs as the PS activator into the advanced oxidation process (AOP) system, the electron transfer of Mn(III/IV) and Fe(III/II) on the surface of MNCs was realized, thus greatly improving the reaction efficiency.

**Keywords:** persulfate; 2,4-dichlorophenol; Fe<sub>3</sub>O<sub>4</sub>/α-MnO<sub>2</sub> magnetic nanocomposite



**Citation:** Zhao, Y.; Luo, F.; Zhou, R. Preparation of Fe<sub>3</sub>O<sub>4</sub>/α-MnO<sub>2</sub> Magnetic Nanocomposites for Degradation of 2,4-DCP through Persulfate Activation. *Water* **2022**, *14*, 3312. <https://doi.org/10.3390/w14203312>

Academic Editors: Jiangshan Li, Xiao Yang and Fei Wang

Received: 28 September 2022

Accepted: 18 October 2022

Published: 20 October 2022

**Publisher's Note:** MDPI stays neutral with regard to jurisdictional claims in published maps and institutional affiliations.



**Copyright:** © 2022 by the authors. Licensee MDPI, Basel, Switzerland. This article is an open access article distributed under the terms and conditions of the Creative Commons Attribution (CC BY) license (<https://creativecommons.org/licenses/by/4.0/>).

## 1. Introduction

Advanced oxidation processes (AOPs) are a new type of remediation technology developed in recent years that uses free radicals to remove organic pollutants in the environment [1,2]. Hydroxyl radicals (•OH), sulfate radicals (SO<sub>4</sub><sup>•-</sup>), superoxide radical (•O<sub>2</sub><sup>-</sup>) and singlet oxygen (<sup>1</sup>O<sub>2</sub>) have all been shown to be able to effectively degrade organic pollutants in various AOPs systems [3–6]. Compared with the traditional Fenton system and other •OH-based AOPs, SO<sub>4</sub><sup>•-</sup>-based AOPs have obvious advantages. For example, the stability of the commonly used oxidant persulfate (PS) is better than that of H<sub>2</sub>O<sub>2</sub>, the degradation of organic pollutants occurs under pH conditions [7], and the lifetime of SO<sub>4</sub><sup>•-</sup> is much longer than that of •OH [8]. Therefore, the application of activated PS-based AOP systems in soil and water remediation has been extensively studied [9–12].

According to the difference in the morphology of SO<sub>4</sub><sup>•-</sup> produced by activated PS, the AOP systems can be divided into homogeneous activation systems and heterogeneous activation systems. Ultraviolet (UV) activation, thermal activation, and transition metal ion activation are commonly used homogeneous activation systems. However, they have significant limitations, such as high cost, strict pH requirements, and secondary pollution. Therefore, heterogeneous activation systems have gradually attracted attention [12]. Among them, iron and manganese oxides are excellent heterogeneous PS activators [8,13]. They can effectively activate PS to produce SO<sub>4</sub><sup>•-</sup> to degrade organic pollutants, and secondary pollution is less likely to occur.

In last few years, magnetic nanoparticles (MNPs) have driven much consideration for several applications. For instance, Ni@SiO<sub>2</sub>-PMo is applied as a recyclable antibacterial agent [14], Fe<sub>3</sub>O<sub>4</sub> MNPs are used as heterogeneous Fenton-like catalysts [15]. Among these MNPs, Fe<sub>3</sub>O<sub>4</sub> can steadily under mild conditions and be easily reused. Besides, Fe<sub>3</sub>O<sub>4</sub> is a mixed-valence iron oxide which Fe(II) species included in its structure can initiate the activation of PS [16]. Some scholars have prepared and modified Fe<sub>3</sub>O<sub>4</sub> magnetic nanomaterials and used Fe(II) to activate PS and effectively degrade organic pollutants, such as 4-aminobenzenesulfonic acid and polychlorinated biphenyls (PCBs) [17,18]. However, due to its magnetic properties, Fe<sub>3</sub>O<sub>4</sub> extremely readily agglomerates, which reduces the number of active sites on the surface. After the reaction, Fe(II) becomes Fe(III), so the efficiency of the activator decreases over time, making the activator less stable and less reusable [13,19]. In addition, Fe<sub>3</sub>O<sub>4</sub> is more effective under acidic conditions, which limits its application.

In recent years, combining the advantages of individual metal compounds to prepare bimetallic core-shell nanomaterials (CSNs) for AOPs has become a popular research topic. Of these compounds, MnO<sub>2</sub> can take different crystal forms, such as  $\alpha$ -,  $\beta$ -,  $\gamma$ -,  $\delta$ -,  $\epsilon$ - and  $\eta$ -. Because these MnO<sub>2</sub> crystal forms can exhibit different heterogeneous activation potentials, they have attracted extensive attention. Among them,  $\alpha$ -MnO<sub>2</sub> with an open  $2 \times 2$  tunnel structure and can facile oxygen vacancy formation on its surface. This characteristic lead to superior catalytic performance compared to other MnO<sub>2</sub> polymorphs in different application, such as the oxygen reduction reaction (ORR), supercapacitors, and heterogeneous catalytic [20]. Xu et al. evaluated the degradation of steroid estrogen with MnO<sub>2</sub> as an activator and showed that MnO<sub>2</sub> is an ideal activator for removing estrogen from water [21]. Edy et al. synthesized different crystalline phases of MnO<sub>2</sub> and tested their heterogeneous activation of PS to degrade phenol [22]. Tushar Kanti Das, et al. synthesized single-layer  $\delta$ -phase MnO<sub>2</sub> nanosheet nanocatalyst toward environmental remediation of hazardous nitroaryl compounds [23]. Although MnO<sub>2</sub> has a good catalytic effect on PS, its lack of magnetism leads to difficulties in recovery and reuse. Theoretically, combining the excellent performance of MnO<sub>2</sub>-activated PS with the advantages of Fe<sub>3</sub>O<sub>4</sub> magnetic recovery, the synthesis of Fe<sub>3</sub>O<sub>4</sub>-MnO<sub>2</sub> CSNs can simultaneously make up for the shortcomings and deficiencies of the two materials. However, the conditions for the synthesis of a certain CSN are relatively harsh and difficult to control, resulting in an increase in cost. Importantly, wrapped by MnO<sub>2</sub>, the Fe<sub>3</sub>O<sub>4</sub> nucleus can play only a role in electron transfer, which is not convenient for direct activation of PS to remove organic pollutants. The use of a simple coprecipitation method to dispersedly load Fe<sub>3</sub>O<sub>4</sub> particles on MnO<sub>2</sub> is a convenient way, which can not only exploit the catalytic performance of MnO<sub>2</sub> but also achieve magnetic recovery.

In view of this, in this study, Fe<sub>3</sub>O<sub>4</sub> MNPs were loaded on  $\alpha$ -MnO<sub>2</sub> nanowires by the hydrothermal synthesis method combined with the ultrasonic coprecipitation method to synthesize Fe<sub>3</sub>O<sub>4</sub>/ $\alpha$ -MnO<sub>2</sub> magnetic nanocomposites (MNCs), an activated PS-based AOP system was constructed using the MNCs, and the degradation efficiency of 2,4-dichlorophenol (2,4-DCP) by this system was investigated.

## 2. Materials and Methods

### 2.1. Reagents and Instruments

Main reagents: 2,4-DCP was purchased from Sigma-Aldrich (Shanghai, China) Trading Co., Ltd. Sodium PS was purchased from Shanghai Aladdin Biochemical Technology Co., Ltd. Ferrous sulfate, ferric chloride, potassium permanganate, hydrochloric acid, acetic acid, ammonia, and other reagents were purchased from Sinopharm Chemical Reagent Co., Ltd. (Shanghai, China). The reagents used in the experiment were all analytically pure, and all solutions were prepared with ultrapure water.

Main instruments: tube furnace (SG-GL1400K, Shanghai Institute of Optics and Fine Mechanics, Shanghai, China), vacuum drying oven (BZF-30, Shanghai Boxun Medical Biological Instrument Corp., Shanghai, China), high-resolution transmission electron mi-

croscope (HRTEM, Tecnai G2 F20 S-TWIN, Thermo Fisher Scientific, Shanghai, China), and UV Spectrophotometer (722 N, Shanghai Precision and Scientific Instrument Corp., Shanghai, China) with wavelength ranging from 250 nm to 800 nm.

## 2.2. Experimental Methods

**Preparation of  $\alpha$ -MnO<sub>2</sub> nanowires:** The  $\alpha$ -MnO<sub>2</sub> nanowires were prepared using an improved hydrothermal synthesis method [24]. First, 0.16 g of KMnO<sub>4</sub> was dissolved in 40 mL of ultrapure water, and 0.7 mL of CH<sub>3</sub>COOH was slowly added dropwise under ultrasonication. The mixed solution was transferred to an autoclave lined with polytetrafluoroethylene, which was sealed and heated to 140 °C. After 12 h, the cooled product was washed several times with ultrapure water and ethanol, placed in a vacuum drying oven, and dried at 60 °C for 8 h. Using this synthesis method, 0.05 g of  $\alpha$ -MnO<sub>2</sub> could be prepared each time. The  $\alpha$ -MnO<sub>2</sub> black powder obtained from several preparations was ground, mixed, and set aside for use.

**Preparation of Fe<sub>3</sub>O<sub>4</sub>/ $\alpha$ -MnO<sub>2</sub> MNC:** The Fe<sub>3</sub>O<sub>4</sub> MNPs were loaded on the  $\alpha$ -MnO<sub>2</sub> nanowires by the ultrasonic coprecipitation method, and the preparation process was carried out under the nitrogen protection. First, for bottle A, 2.705 g of FeCl<sub>3</sub>·6H<sub>2</sub>O and 20 mL of oxygen-free water were added, two drops of (1 + 1) HCl were added, and 2.780 g of FeSO<sub>4</sub>·7H<sub>2</sub>O was added. The mixture was shaken until the solids dissolved. Bottle B was placed in a 70 °C water bath/ultrasonic generator at 40 Hz. For bottle B, the prepared  $\alpha$ -MnO<sub>2</sub> and 30 mL of oxygen-free water were first added, and 10 mL of concentrated ammonia was added after 10 min. The liquid in bottle A was added dropwise to bottle B. After 1 h, bottle B was removed from the ultrasonic generator and shaken in an air shaker for 12 h. Finally, the prepared nanomaterials were washed with oxygen-free water and ethanol until they were neutral. The obtained composites were dried in a tube furnace at 80 °C for 4 h under the nitrogen protection. After drying, the products were ground in a vacuum bag with an agate mortar to a fine powder, i.e., the Fe<sub>3</sub>O<sub>4</sub>/ $\alpha$ -MnO<sub>2</sub> MNCs. The MNCs were sealed in a glass bottle filled with nitrogen and stored in a refrigerator. During the preparation process, MNCs with different iron and manganese ratios were obtained by adjusting the amount of  $\alpha$ -MnO<sub>2</sub>.

**Experimental procedure:** A certain amount of Fe<sub>3</sub>O<sub>4</sub>/ $\alpha$ -MnO<sub>2</sub> MNCs and 2,4-DCP stock solution were sequentially added to the reaction vessel and ultrasonically dispersed. After the ultrasonication feature was turned off, an amount of PS stock solution was added to trigger the activation reaction, with shaking at a constant temperature. At different times, 0.2 mL liquid samples were taken from the reaction vessel, and excess methanol was added to quench the free radical reaction. The mixture of water and methanol mixture was then passed through a 0.22  $\mu$ m filter membrane and used for the 2,4-DCP determination.

## 2.3. Analysis Methods

The 2,4-DCP was measured by spectrophotometry [25]. A 600  $\mu$ L liquid sample was placed in a 10 mL colorimetric detector tube, and 100  $\mu$ L of 20.8 mM 4-aminoantipyrine solution, 100  $\mu$ L of 83.4 mM potassium ferricyanide solution, and 200  $\mu$ L of 0.25 M sodium bicarbonate solution (pH = 8.4) were added. After ultrapure water was added until the marked line was reached, the color was developed for 10 min, the solution was transferred to a 10 mm cuvette, and the optical density (OD) was measured at 510 nm using a spectrophotometer. The standard solution was prepared using the same procedure, and the standard curve was drawn after the measurement.

## 3. Results and Discussion

### 3.1. Characterization of the Fe<sub>3</sub>O<sub>4</sub>/ $\alpha$ -MnO<sub>2</sub> MNCs

The X-ray diffraction (XRD) results of the Fe<sub>3</sub>O<sub>4</sub>/ $\alpha$ -MnO<sub>2</sub> MNCs are shown in Figure 1a. In the scanning range of 10°–90°, the characteristic peaks match the peaks of Fe<sub>3</sub>O<sub>4</sub> and (44-0141)  $\alpha$ -MnO<sub>2</sub> in JCPDS card (19-0629) [15,26], proving that the synthesized MNCs are composed of Fe<sub>3</sub>O<sub>4</sub> and  $\alpha$ -MnO<sub>2</sub>.

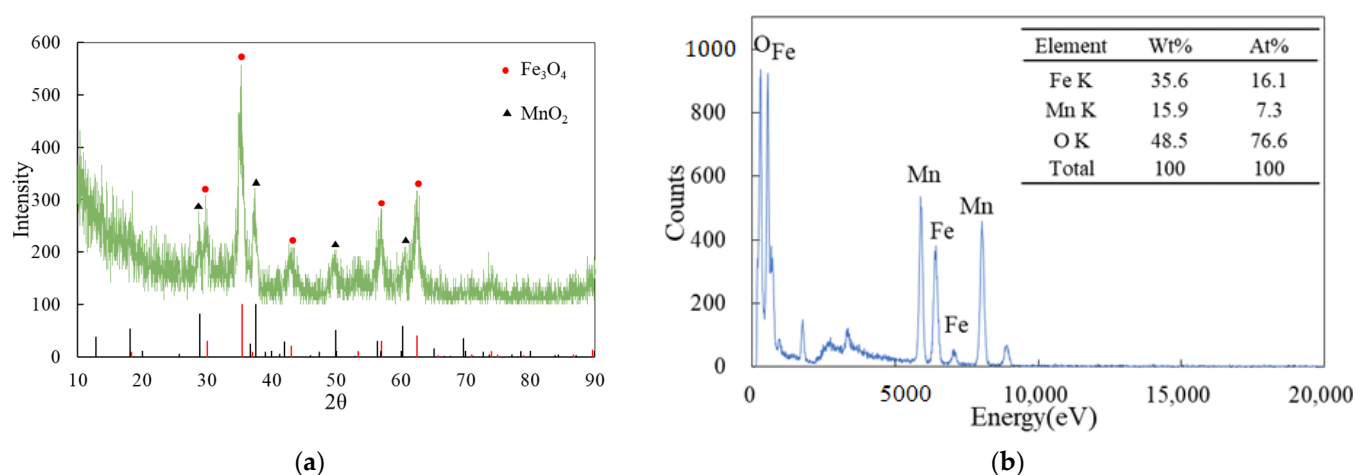


**Figure 1.** (a) X-ray diffraction pattern of  $\text{Fe}_3\text{O}_4/\text{MnO}_2$  (the green line represents the XRD of  $\text{Fe}_3\text{O}_4/\text{MnO}_2$ , the red lines represent the characteristic peaks of  $\text{Fe}_3\text{O}_4$ , and the black lines represent the characteristic peaks of  $\alpha\text{-MnO}_2$ ); (b) EDX of  $\text{Fe}_3\text{O}_4/\text{MnO}_2$ .

The elemental composition of the  $\text{Fe}_3\text{O}_4/\alpha\text{-MnO}_2$  MNCs was analyzed using energy dispersive X-ray (EDX) microanalysis. The ratio of  $\text{Fe}_3\text{O}_4$  to  $\alpha\text{-MnO}_2$  in the measured samples is 0.7 to 1, and results are shown in Figure 1b. In the EDX spectrum, the measured ratios of Fe and Mn are similar to those during the preparation; the molar percentages of Fe and Mn are 16.1% and 7.3%, and the mass percentages are 35.6% and 15.9%, respectively.

The  $\text{Fe}_3\text{O}_4/\alpha\text{-MnO}_2$  MNCs were characterized by HRTEM, and the results are shown in Figure 2a–d. As shown in the figure, the diameter of  $\text{Fe}_3\text{O}_4$  MNPs is approximately 20 nm, and the width of  $\alpha\text{-MnO}_2$  nanowires is 10 nm–50 nm. The  $\text{Fe}_3\text{O}_4$  MNPs are dispersedly loaded on the  $\alpha\text{-MnO}_2$  nanowires, so the dispersion of the  $\text{Fe}_3\text{O}_4$  MNPs is improved and the  $\alpha\text{-MnO}_2$  nanowires can be exposed, which can help the two materials simultaneously perform activation.

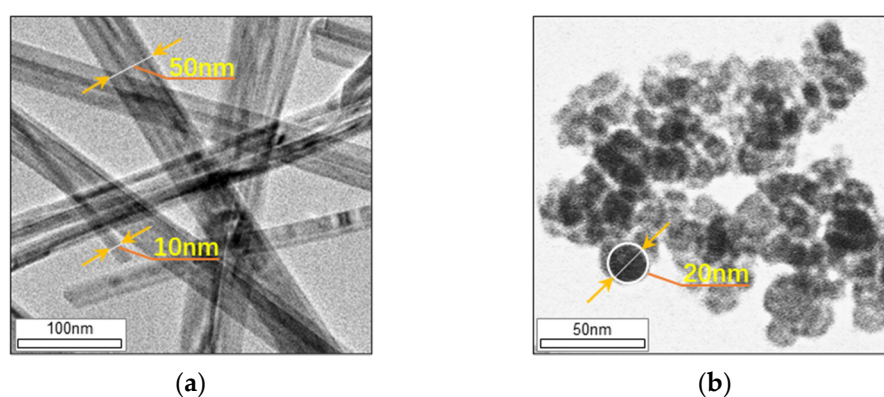


**Figure 2.** Cont.

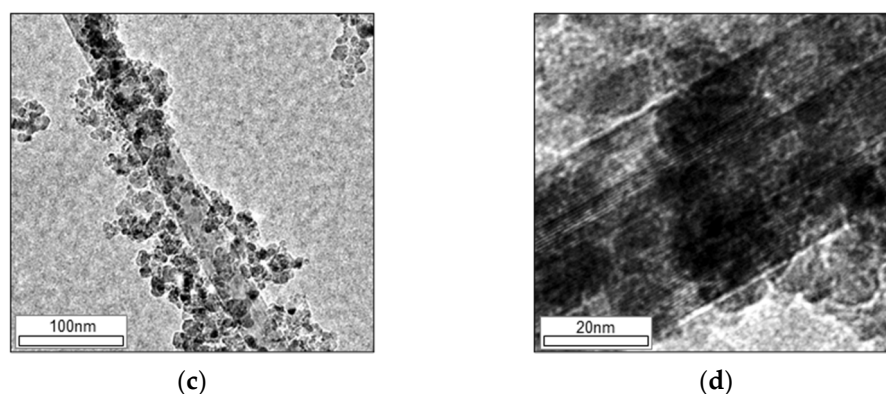


**Figure 2.** TEM images of (a)  $\alpha$ -MnO<sub>2</sub>; (b) Fe<sub>3</sub>O<sub>4</sub> MNPs; (c) Fe<sub>3</sub>O<sub>4</sub>/ $\alpha$ -MnO<sub>2</sub>; (d) HRTEM image of Fe<sub>3</sub>O<sub>4</sub>/ $\alpha$ -MnO<sub>2</sub>.

### 3.2. Effectiveness of the Fe<sub>3</sub>O<sub>4</sub>/ $\alpha$ -MnO<sub>2</sub> MNCs in the Removal of 2,4-DCP by PS Activation

#### 3.2.1. Comparison of 2,4-DCP Removal by Different Activated PS-Based Systems

The removal of 2,4-DCP in different systems was compared to verify the effectiveness of Fe<sub>3</sub>O<sub>4</sub>/ $\alpha$ -MnO<sub>2</sub> MNCs. Systems with only PS, only Fe<sub>3</sub>O<sub>4</sub>/ $\alpha$ -MnO<sub>2</sub> MNCs, and both PS and Fe<sub>3</sub>O<sub>4</sub>/ $\alpha$ -MnO<sub>2</sub> MNCs were prepared. The concentration of PS added was 30 mM, the dosage of MNCs was 0.4 g/L, the initial concentration of 2,4-DCP was 100 mg/L, the initial pH was 7, and the temperature was 30 °C. The changes in the concentration of 2,4-DCP in each system within 180 min of the reaction are shown in Figure 3. When only the oxidant PS or the activator Fe<sub>3</sub>O<sub>4</sub>/ $\alpha$ -MnO<sub>2</sub> MNC is added, the final removal rate of 2,4-DCP is only 3.1% and 1.5%, respectively. These results indicate that the pollutants adsorbed by the PS direct oxidation and Fe<sub>3</sub>O<sub>4</sub>/ $\alpha$ -MnO<sub>2</sub> MNCs are negligible. In the Fe<sub>3</sub>O<sub>4</sub>/ $\alpha$ -MnO<sub>2</sub>-activated PS system, the degradation rate of 2,4-DCP reaches 96.3%, which is much higher than that of the other two systems. This result shows that the prepared Fe<sub>3</sub>O<sub>4</sub>/ $\alpha$ -MnO<sub>2</sub> MNCs can effectively activate PS to remove 2,4-DCP.

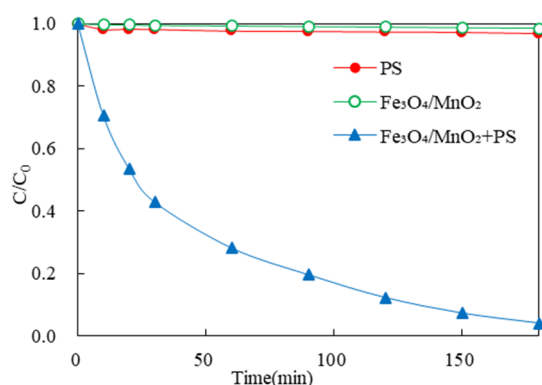


**Figure 3.** Effectiveness of Fe<sub>3</sub>O<sub>4</sub>/ $\alpha$ -MnO<sub>2</sub> MNCs.

#### 3.2.2. Optimization of the Loading Ratio of Fe<sub>3</sub>O<sub>4</sub> on $\alpha$ -MnO<sub>2</sub>

Fe<sub>3</sub>O<sub>4</sub>/ $\alpha$ -MnO<sub>2</sub> MNCs with molar ratios of Fe<sub>3</sub>O<sub>4</sub> MNPs and  $\alpha$ -MnO<sub>2</sub> nanowires of 0.5:1, 0.7:1, 1:1, 2:1, and 5:1 were prepared, and the effectiveness of these 5 types of Fe<sub>3</sub>O<sub>4</sub>/ $\alpha$ -MnO<sub>2</sub> MNCs in activating PS to degrade 2,4-DCP was investigated. The results are shown in Figure 4. At 30 °C, the PS concentration was 30 mM, the concentration of Fe<sub>3</sub>O<sub>4</sub>/ $\alpha$ -MnO<sub>2</sub> MNCs is 0.4 g/L, the 2,4-DCP concentration is 100 mg/L, and the pH is 7. After 180 min of reaction, the removal rates of 2,4-DCP by degradation are 92.1%, 96.3%, 83.7%, 66.8%, and 52.7% for the above 5 Fe<sub>3</sub>O<sub>4</sub>/ $\alpha$ -MnO<sub>2</sub> MNCs, respectively. The results show that when the molar ratio of Fe<sub>3</sub>O<sub>4</sub> to  $\alpha$ -MnO<sub>2</sub> is 0.7:1, the Fe<sub>3</sub>O<sub>4</sub>/ $\alpha$ -MnO<sub>2</sub> MNC show the best effectiveness in terms of the degradation of 2,4-DCP by activating PS. When the proportion of Fe<sub>3</sub>O<sub>4</sub> is further increased, the activation ability of the activator worsens.

On the one hand, the results in 3.5.1 show that the activation ability of  $\alpha$ -MnO<sub>2</sub> nanowires is better than that of Fe<sub>3</sub>O<sub>4</sub> MNPs of the same mass, and a high molar ratio of Fe<sub>3</sub>O<sub>4</sub> MNPs and  $\alpha$ -MnO<sub>2</sub> indicates the low  $\alpha$ -MnO<sub>2</sub> proportion in the prepared MNCs, which decreases the activation performance of the MNCs. Moreover, MnO<sub>2</sub> nanowires support the Fe<sub>3</sub>O<sub>4</sub> MNPs as the skeleton, which enhance the dispersion and reduce the aggregation effect of Fe<sub>3</sub>O<sub>4</sub> MNPs. Herein, more activated sites on the surface of Fe<sub>3</sub>O<sub>4</sub>/ $\alpha$ -MnO<sub>2</sub> MNCs are exposed to enhance the activation performance of the MNCs. Similar phenomenon has been observed in other scholars' studies [27,28]. Wu et al. improved the problem of agglomeration by synthesizing composite material of D-ATP-nFe/Ni, which also utilizes the support function of the attapulgite to weaken the aggregation effect of Fe/Ni bimetallic nanoparticles [28]. On the contrary, due to the agglomeration of Fe<sub>3</sub>O<sub>4</sub>, a high molar ratio for Fe<sub>3</sub>O<sub>4</sub> MNPs in the prepared MNCs can easily lead to uneven dispersion of MNPs on  $\alpha$ -MnO<sub>2</sub> nanowires, or even the complete coverage of  $\alpha$ -MnO<sub>2</sub> nanowires by excessive MNPs. These two effects reduce the number of activated sites on the MNCs and lead to a reduction in 2,4-DCP removal. On the other hand, a low molar ratio for Fe<sub>3</sub>O<sub>4</sub> MNPs and  $\alpha$ -MnO<sub>2</sub> may affect the synergistic catalytic effect between Fe<sub>3</sub>O<sub>4</sub> and  $\alpha$ -MnO<sub>2</sub>, thus reducing the removal rate of 2,4-DCP. Based on the experimental results, Fe<sub>3</sub>O<sub>4</sub>/ $\alpha$ -MnO<sub>2</sub> MNCs prepared with a molar ratio of 0.7:1 between Fe<sub>3</sub>O<sub>4</sub> and  $\alpha$ -MnO<sub>2</sub> were used as activators in subsequent experiments.

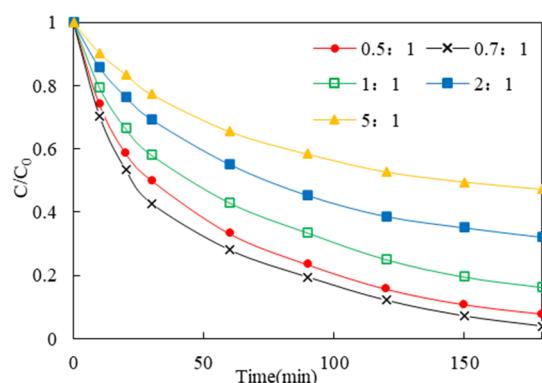


**Figure 4.** Influence of various Fe<sub>3</sub>O<sub>4</sub> and  $\alpha$ -MnO<sub>2</sub> molar ratios on the degradation of 2,4-DCP.

### 3.3. Influencing Factors of 2,4-DCP Removal through the Activated PS by Fe<sub>3</sub>O<sub>4</sub>/ $\alpha$ -MnO<sub>2</sub> MNCs

#### 3.3.1. Effect of Activator Dosage

The effect of Fe<sub>3</sub>O<sub>4</sub>/ $\alpha$ -MnO<sub>2</sub> MNCs on the removal efficiency of 2,4-DCP was investigated at 30 °C, PS concentration of 30 mM, 2,4-DCP concentration of 100 mg/L, and pH of 7. The results are shown in Figure 5a. The activator concentrations were 0.1–0.8 g/L. After 180 min of reaction, the removal rates of 2,4-DCP are 50.9%, 61.6%, 96.3%, 90.3%, and 79.6%, respectively. As the dosage of activator increases from 0.1 g/L to 0.4 g/L, the degradation rate of 2,4-DCP increases accordingly; however, as the dosage of activator continues to increase from 0.4 g/L to 0.8 g/L, the removal rate of 2,4-DCP decreases instead.

In the Fe<sub>3</sub>O<sub>4</sub>/ $\alpha$ -MnO<sub>2</sub>-activated PS system, both Fe<sub>3</sub>O<sub>4</sub> and  $\alpha$ -MnO<sub>2</sub> can activate PS to generate free radicals to degrade and remove 2,4-DCP. Previous studies have shown that when  $\alpha$ -MnO<sub>2</sub> alone is used to activate PS, an increase in activator dosage does not lead to a decrease in pollutant removal and reaction rate [29]. While Fe<sub>3</sub>O<sub>4</sub> alone is used to activate PS, the results are similar to those of this study [15,30]. Therefore, with a further increase in the activator dosage, the decrease in the 2,4-DCP removal rate is caused by the excess of Fe<sub>3</sub>O<sub>4</sub>. On the one hand, Fe<sub>3</sub>O<sub>4</sub> provides Fe(II) to activate PS, but with further increase in Fe<sub>3</sub>O<sub>4</sub> concentration, Fe(II) also increases, and consequently, more SO<sub>4</sub><sup>-•</sup> is produced. The excess Fe(II), PS and SO<sub>4</sub><sup>-•</sup> all have a quenching effect on SO<sub>4</sub><sup>-•</sup> [31], resulting in less SO<sub>4</sub><sup>-•</sup> in the system to participate in the oxidative degradation of 2,4-DCP, which causes a decrease in the removal rate of 2,4-DCP. On the other hand, due to the magnetic properties of the Fe<sub>3</sub>O<sub>4</sub>/ $\alpha$ -MnO<sub>2</sub> MNCs, excessive dosage would lead to agglomeration

of the activator, which would affect the contact area between the PS and the activator, resulting in a decrease in the removal rate of 2,4-DCP.

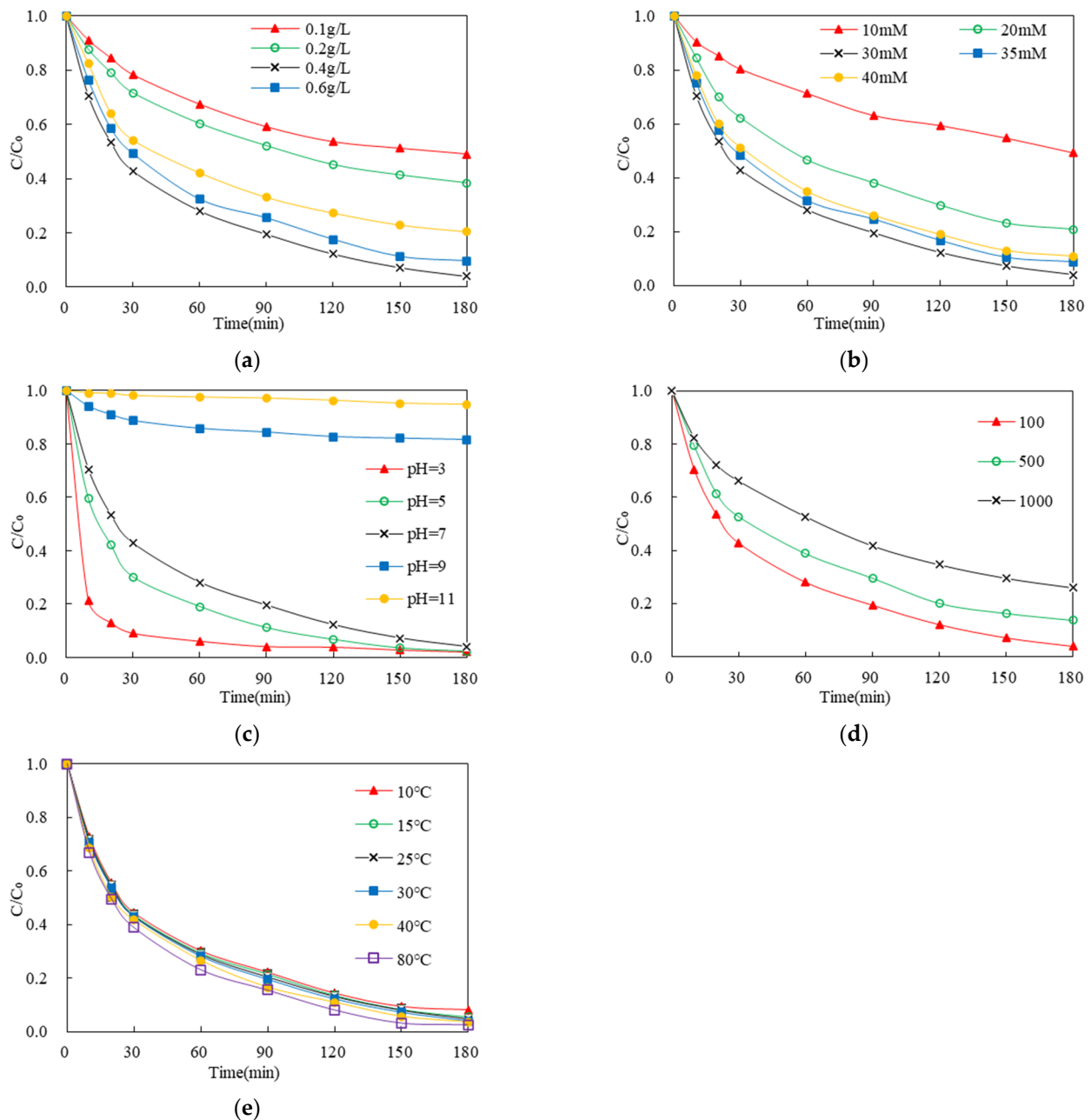


**Figure 5.** Influence of (a) catalyst dose; (b) PS concentration; (c) initial pH; (d) initial 2,4-DCP concentration; (e) temperature on degradation of 2,4-DCP.

The results showed that when the dosage of the activator  $\text{Fe}_3\text{O}_4/\alpha\text{-MnO}_2$  is 0.4 g/L, the degradation rate of 2,4-DCP is the highest. After 180 min of reaction, the removal rate of 2,4-DCP reaches the highest rate, of 96.3%. Therefore, an activator dosage of 0.4 g/L was used in subsequent experiments.

### 3.3.2. Effect of Oxidant Dosage

Systems with 10–40 mM PS were prepared, and other experimental conditions were as follows: the initial 2,4-DCP concentration was 100 mg/L, the dosage of  $\text{Fe}_3\text{O}_4/\alpha\text{-MnO}_2$  MNCs was 0.4 g/L, the reaction temperature was 30 °C, and the initial pH was 7. Figure 5b

shows that, as the PS concentration increases from 10 mM to 40 mM, after 180 min of reaction, the removal rates of 2,4-DCP are 50.7%, 79.1%, 96.3%, 91.3%, and 89.1%, respectively. With increasing PS dosage, the removal rate shows a trend of first increasing and then decreasing. The highest removal rate of 2,4-DCP by the  $\text{Fe}_3\text{O}_4/\alpha\text{-MnO}_2$ -activated PS system is reached when the PS concentration is 30 mM.

When the PS concentration is too high, the reaction system can generate a large amount of  $\text{SO}_4^{\cdot-}$  in a short time, and the high concentration of  $\text{SO}_4^{\cdot-}$  can cause a self-quenching reaction ( $K = 8.9 \times 10^8 \text{ M}^{-1}\cdot\text{s}^{-1}$ ) [32]. At the same time, excessive PS can also become the quencher of  $\text{SO}_4^{\cdot-}$  [27]. Therefore, the concentration and the effective utilization rate of  $\text{SO}_4^{\cdot-}$  are reduced, resulting in decreases in the removal rates of 2,4-DCP.

The above two experimental results show that for the 2,4-DCP solution with a concentration of 100 mg/L, when the dosage of  $\text{Fe}_3\text{O}_4/\alpha\text{-MnO}_2$  MNCs is 0.4 g/L and the initial concentration of PS is 30 mM, the degradation rate of 2,4-DCP reaches 96.3% after 180 min of reaction. Therefore,  $\text{Fe}_3\text{O}_4/\alpha\text{-MnO}_2$  MNCs (activator) of 0.4 g/L and the initial PS (oxidant) concentration of 30 mM are used in subsequent experiments.

### 3.3.3. The Effect of the Initial pH of the System

Systems with initial pH values of 3, 5, 7, 9 and 11 were prepared to investigate the effect of the initial pH of the system on the removal of 2,4-DCP, and the other reaction conditions were as follows: the dosage of  $\text{Fe}_3\text{O}_4/\alpha\text{-MnO}_2$  MNCs was 0.4 g/L, the initial concentration of PS was 30 mM, the initial concentration of 2,4-DCP was 100 mg/L, and the temperature was 30 °C. As shown in Figure 5c, after 180 min of reaction, the removal rates of 2,4-DCP are 97.9%, 97.6%, 96.3%, 18.4%, and 5.2%, respectively. The lower the pH is, the better the removal of 2,4-DCP and the faster the degradation rate. When the initial pH is 3, the removal rate of 2,4-DCP reaches 86.9% at 20 min. With increasing pH, the reaction rate observed decreases. When the pH is neutral, the removal rate of 2,4-DCP reaches 87.8% at 120 min, which is closely to that under acid condition (pH = 3) in 20 min. Under alkaline conditions, the oxidative capacity of the  $\text{Fe}_3\text{O}_4/\alpha\text{-MnO}_2$ -activated PS system is inhibited, and the removal rate of 2,4-DCP decreased to less than 20% in 180 min. In addition, although the reaction rate observed under pH = 3, 5, and 7 are different at the beginning of the experiment, the difference in the removal rate of 2,4-DCP after 180 min is less than 1%. This phenomenon indicates that under acidic and neutral initial conditions, the  $\text{Fe}_3\text{O}_4/\alpha\text{-MnO}_2$ -activated PS system can effectively degrade 2,4-DCP.

Studies have shown that the redox conditions of  $\text{S}_2\text{O}_8^{2-}$  are different in acidic, neutral, and alkaline environments and that the free radicals that degrade pollutants in the system are different. When pH is approximately 2–7,  $\text{SO}_4^{\cdot-}$  is the dominant active free radical; when pH is approximately 9,  $\text{SO}_4^{\cdot-}$  and  $\bullet\text{OH}$  coexist; when pH > 12,  $\bullet\text{OH}$  is the dominant active free radical [33]. Studies have shown that when pH is low, the formation of  $\text{SO}_4^{\cdot-}$  by  $\text{S}_2\text{O}_8^{2-}$  can be accelerated under acid catalysis [34], which may increase the degradation rate of pollutants. The acidic environment (low pH) can also lead to the dissolution of  $\text{Fe}^{2+}$  in the  $\text{Fe}_3\text{O}_4/\alpha\text{-MnO}_2$  MNCs, thereby increasing the removal rate of 2,4-DCP.

When pH = 7, the degradation rate of 2,4-DCP is 96.3% at 180 min, and when the pH continues to increase to 9 and 11, the degradation rates of 2,4-DCP are only 18.4% and 5.2% at 180 min, respectively. As the pH increases,  $\bullet\text{OH}$  becomes the main active free radical, while the decomposition of  $\text{H}_2\text{O}_2$  and the quenching of  $\text{SO}_4^{\cdot-}$  and  $\bullet\text{OH}$  under alkaline conditions reduce the amount of  $\bullet\text{OH}$ . Meanwhile the redox potential of  $\bullet\text{OH}$  decreases with increasing pH. These two effects result in a decrease in the removal rate of pollutants [35].

The surface charge of  $\alpha\text{-MnO}_2$  may also be one of the influencing factors. Previous studies have shown that the electrical properties of the surface charge of metal oxides are related to the pH of the solution at the point of zero charge ( $\text{pH}_{\text{pzc}}$ ) [36,37]. When  $\text{pH} < \text{pH}_{\text{pzc}}$ , metal oxides have a positive surface charge; when  $\text{pH} > \text{pH}_{\text{pzc}}$ , metal oxides have a negative surface charge. Pr elot et al. reported the  $\text{pH}_{\text{pzc}}$  of several manganese oxides, including the  $\text{pH}_{\text{pzc}}$  of  $\alpha\text{-MnO}_2 = 4.5/4.6$  [38]. When  $\text{pH} = 3$ , i.e.,  $\text{pH} < \text{pH}_{\text{pzc}}$ , the

surface of  $\alpha$ -MnO<sub>2</sub> is positively charged. Due to the attraction of unlike charges, S<sub>2</sub>O<sub>8</sub><sup>2-</sup> is more likely to move to the surface of the activator to generate free active radicals to oxidatively degrade 2,4-DCP. When pH = 5–11, i.e., pH > p*H*<sub>pzc</sub>, the surface of  $\alpha$ -MnO<sub>2</sub> is negatively charged. Due to the repulsion of the like charges, the contact of S<sub>2</sub>O<sub>8</sub><sup>2-</sup> with the surface of the activator is blocked, resulting in the inhibition of the free active radical production [37], so the removal rate of 2,4-DCP decreases.

#### 3.3.4. Effect of Initial Pollutant Concentration in the System

Systems with initial 2,4-DCP concentrations of 100, 500, and 1000 mg/L were prepared to investigate the effect of the initial 2,4-DCP concentration on the activation. The other reaction conditions were as follows: the dosage of Fe<sub>3</sub>O<sub>4</sub>/ $\alpha$ -MnO<sub>2</sub> MNCs was 0.4 g/L, the initial concentration of PS was 30 mM, the initial pH was 7, and the temperature was 30 °C. As shown in Figure 5d, after 180 min of reaction, the removal rates of 2,4-DCP are 96.3%, 86.3%, and 74.1%, respectively, indicating that with an increasing initial concentration of 2,4-DCP, the removal rate gradually decreases. When the pollutant concentration is too high, the system cannot generate enough active free radicals to degrade and remove pollutants when the amount of added oxidizer and activator is a constant.

#### 3.3.5. Effect of Temperature

Systems with temperatures of 10 °C, 15 °C, 25 °C, 30 °C, 40 °C and 80 °C were prepared to investigate the effect of system temperature on the removal of 2,4-DCP, and other reaction conditions were as follows: the dosage of Fe<sub>3</sub>O<sub>4</sub>/ $\alpha$ -MnO<sub>2</sub> MNCs was 0.4 g/L, the initial concentration of PS was 30 mM, the initial pH was 7, and the initial concentration of 2,4-DCP was 100 mg/L. Figure 5e shows that under the experimental conditions of this study, as the temperature decreases from 80 °C to 10 °C, the removal rate of 2,4-DCP decreases from 97.4% to 91.9% at 180 min. The removal rate decreases by only 5.5% when the temperature decreases by 70 °C. This result indicates the Fe<sub>3</sub>O<sub>4</sub>/ $\alpha$ -MnO<sub>2</sub>-activated PS system for 2,4-DCP degradation is not sensitive to the reaction temperature. Therefore, this system can be applied in both high and low-temperature environments and can still effectively degrade pollutants. In particular, compared with other activated PS systems for degradation of organic pollutants, the Fe<sub>3</sub>O<sub>4</sub>/ $\alpha$ -MnO<sub>2</sub> MNCs are found to have excellent activation performance for PS in a low-temperature environment [19,39]. Temperature has a weaker effect on the degradation rate than the oxidant dosage, activator dosage, initial pH, and initial pollutant concentration; i.e., the system is the least sensitive to the influencing factor of temperature.

#### 3.4. Reusability

The Fe<sub>3</sub>O<sub>4</sub>/ $\alpha$ -MnO<sub>2</sub> MNCs were recovered and repeatedly added to the reaction system under the same initial conditions to investigate their reusability. The reaction conditions were as follows: the temperature was 30 °C, the PS concentration was 30 mM, the dosage of Fe<sub>3</sub>O<sub>4</sub>/ $\alpha$ -MnO<sub>2</sub> MNCs was 0.4 g/L, the initial 2,4-DCP concentration was 100 mg/L, and the initial pH was 7. Figure 6 shows that after four repeated uses, the Fe<sub>3</sub>O<sub>4</sub>/ $\alpha$ -MnO<sub>2</sub> MNCs still had good activation performance, and the degradation rate of 2,4-DCP reached 94.0%, which is only 2.0% lower than that of the first use, indicating that the Fe<sub>3</sub>O<sub>4</sub>/ $\alpha$ -MnO<sub>2</sub> MNCs have excellent reusability.

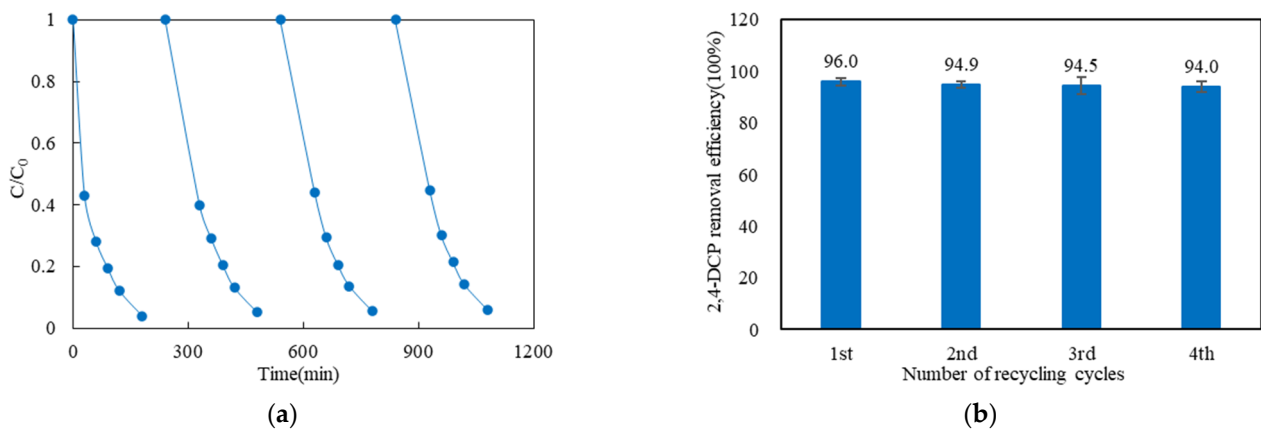


**Figure 6.** Reuse of the catalyst (a) Degradation of 2,4-DCP; (b) Removal efficiency of 2,4-DCP.

### 3.5. Reaction Mechanism of 2,4-DCP Removal by the $Fe_3O_4/\alpha-MnO_2$ -Activated PS System

#### 3.5.1. Comparison of 2,4-DCP Removal by Different Activated PS Systems

The removal of 2,4-DCP in different systems was compared. The four systems were as follows: ①  $Fe_3O_4$  MNPs + PS, ②  $\alpha-MnO_2$  nanowires + PS, ③  $Fe_3O_4$  MNPs +  $\alpha-MnO_2$  nanowires + PS, and ④  $Fe_3O_4/\alpha-MnO_2$  MNCs + PS. The concentration of the solid activator in the system was 0.4 g/L, the concentration of PS was 30 mM, the initial concentration of 2,4-DCP was 100 mg/L, the initial pH was 7, and the temperature was 30 °C. The variation in 2,4-DCP concentration with time for each system within 180 min is shown Figure 7. For systems ① and ②, the removal rates are 47.4% and 66.4%, respectively, indicating that both can effectively activate PS to remove 2,4-DCP in water. At the same dosage, the activation effect of  $\alpha-MnO_2$  nanowires on PS is better than that of  $Fe_3O_4$  MNPs. For system ③, the 2,4-DCP removal rate is 53.3%, which is in between those of systems ① and ②, indicating that physical mixing of the activators and oxidant cannot significantly increase the activation capacity of the system. For system ④, the degradation rate of 2,4-DCP reaches 96.3%, which is much higher than that of other systems, indicating that for the  $Fe_3O_4/\alpha-MnO_2$  MNCs prepared by the hydrothermal synthesis method and the ultrasonic coprecipitation method, the activation capacity is significantly improved, and the activation performance is much better than that of the systems ① ( $Fe_3O_4$  MNPs alone), ② ( $\alpha-MnO_2$  nanowires alone) and ③ (mixture of  $Fe_3O_4$  and  $\alpha-MnO_2$ ), indicating that there is a synergistic catalytic effect between  $Fe_3O_4$  and  $\alpha-MnO_2$  in the MNCs. Similar synergistic effects due to electron transfer have been found in other studies [40,41]. In addition, in the process of multiple recycling and reuse cycles, the  $Fe_3O_4/\alpha-MnO_2$  MNCs still maintain high activation performance, indicating that in the process of activating PS to degrade pollutants, the leaching effect is limited, and the reaction mainly occurs on the surface of the MNCs.

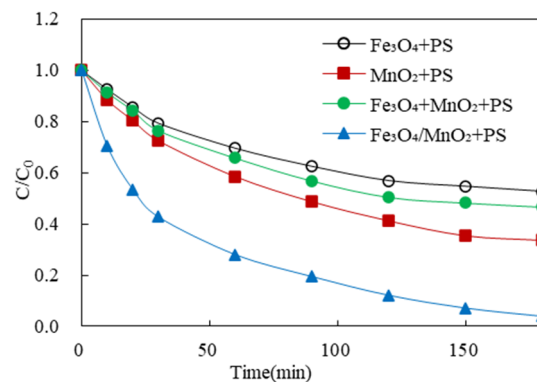


**Figure 7.** Degradation of 2,4-DCP in different systems.

### 3.5.2. Speculation of the Reaction Mechanism for the Removal of 2,4-DCP by the Fe<sub>3</sub>O<sub>4</sub>/α-MnO<sub>2</sub>-Activated PS System

The speculated mechanism for the removal of 2,4-DCP by the Fe<sub>3</sub>O<sub>4</sub>/α-MnO<sub>2</sub>-activated PS system based on the experimental results is shown in Figure 8. In the process of 2,4-DCP degradation by the Fe<sub>3</sub>O<sub>4</sub>/α-MnO<sub>2</sub>-activated PS system, Fe(II) and Mn(IV) on the surface can react with PS to generate free radicals, as shown in Equations (1) and (2).

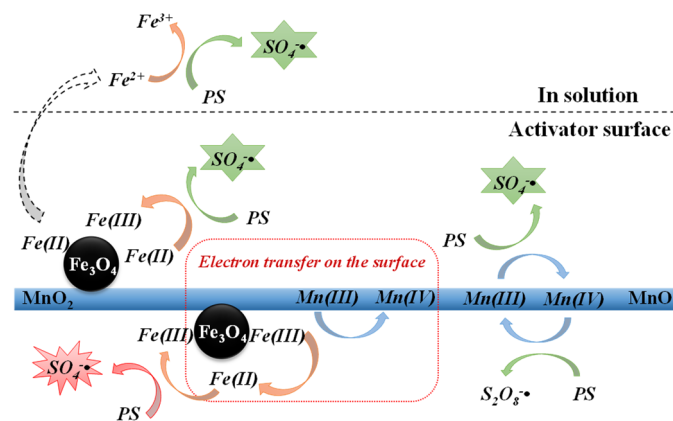
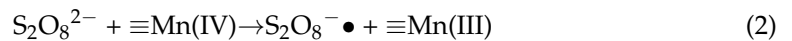
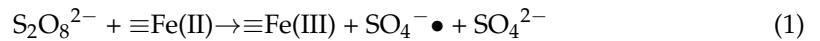


**Figure 8.** Mechanism of Fe<sub>3</sub>O<sub>4</sub>/α-MnO<sub>2</sub> composite activation of PS.

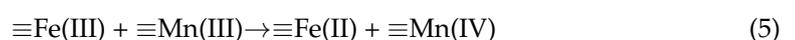
The Mn(III) formed by the reaction of Mn(IV) with PS can continue to activate PS to produce sulfate radicals, as shown in Equation (3).



In addition, a small amount of Fe<sup>2+</sup> leached into the solution can activate PS to produce sulfate radicals, as shown in Equation (4).



These three ways of generating free active radicals are the same as those in the system with the physical mixture of Fe<sub>3</sub>O<sub>4</sub> MNPs, α-MnO<sub>2</sub> nanowires and PS. However, the comparison of the results of different systems shows that the 2,4-DCP removal rate in the Fe<sub>3</sub>O<sub>4</sub>/α-MnO<sub>2</sub> MNCs + PS system is 43% higher than that in the system with the physical mixture of Fe<sub>3</sub>O<sub>4</sub> MNPs, α-MnO<sub>2</sub> nanowires, and PS, indicating that there might be other reactions for radical generation in the Fe<sub>3</sub>O<sub>4</sub>/α-MnO<sub>2</sub>-activated PS system, which enhances the activation performance of the Fe<sub>3</sub>O<sub>4</sub>/α-MnO<sub>2</sub> MNCs, thus increasing the degradation rate of 2,4-DCP. Therefore, it is speculated that in the Fe<sub>3</sub>O<sub>4</sub>/α-MnO<sub>2</sub>-activated PS system, there may be electron transfer between the transition metals on the surface of MNCs, i.e., the Fe(III) and Mn(III) on the surface of MNCs undergo redox reaction to realize electron transfer, Mn(III) loses an electron to produce Mn(IV), and Fe(III) gains an electron to produce Fe(II), as shown in Equation (5).



Therefore, the number of Fe(II) sites on the MNC surface that can activate PS is increased, as illustrated in the dashed box in Figure 8. The electron transfer on the surface may be the reason for the synergistic catalytic effect between Fe<sub>3</sub>O<sub>4</sub> and α-MnO<sub>2</sub> in Fe<sub>3</sub>O<sub>4</sub>/α-MnO<sub>2</sub> MNCs, and this synergistic catalytic effect enhances the activation performance of

Fe<sub>3</sub>O<sub>4</sub>/α-MnO<sub>2</sub> MNCs and significantly improves the degradation rate of the pollutant 2,4-DCP.

#### 4. Conclusions

In this study, a novel Fe<sub>3</sub>O<sub>4</sub>/α-MnO<sub>2</sub> MNCs were prepared by loading Fe<sub>3</sub>O<sub>4</sub> MNPs on α-MnO<sub>2</sub> nanowires by an improved hydrothermal synthesis method combined with an ultrasonic coprecipitation method, and the optimal loading ratio was 0.7:1. The MNCs were characterized by XRD and TEM. The results showed that the Fe<sub>3</sub>O<sub>4</sub>/α-MnO<sub>2</sub> MNCs could effectively activate PS to remove 2,4-DCP from water. Under the present experiment conditions, the degradation rate of 100 mg/L 2,4-DCP reached 96.3% after 180 min of reaction. The possible reaction mechanism of the Fe<sub>3</sub>O<sub>4</sub>/α-MnO<sub>2</sub>-activated PS system for the degradation of 2,4-DCP was described. Electron transfer may occur on the surface of the MNCs to produce a synergistic catalytic effect, which greatly improves the activation performance of the MNCs to PS.

**Author Contributions:** Conceptualization, R.Z. and Y.Z.; methodology, R.Z. and Y.Z.; validation, F.L. and Y.Z.; formal analysis, Y.Z. and R.Z.; investigation, Y.Z. and R.Z.; resources, R.Z.; writing—original draft preparation, Y.Z.; writing—review and editing, R.Z. and Y.Z.; visualization, Y.Z.; supervision, R.Z.; project administration, R.Z. and F.L.; funding acquisition, F.L. All authors have read and agreed to the published version of the manuscript.

**Funding:** This research received no external funding.

**Institutional Review Board Statement:** Not applicable.

**Informed Consent Statement:** Not applicable.

**Data Availability Statement:** The data presented in this study are available on request from the corresponding authors.

**Conflicts of Interest:** The authors declare no conflict of interest.

#### References

1. Ribeiro, A.R.; Nunes, O.C.; Pereira, M.F.R.; Silva, A.M.T. An overview on the advanced oxidation processes applied for the treatment of water pollutants defined in the recently launched Directive 2013/39/EU. *Environ. Int.* **2015**, *75*, 33–51. [[CrossRef](#)]
2. Wang, J.L.; Xu, L.J. Advanced Oxidation Processes for Wastewater Treatment: Formation of Hydroxyl Radical and Application. *Crit. Rev. Environ. Sci. Technol.* **2012**, *42*, 251–325. [[CrossRef](#)]
3. Asgari, E.; Esrafil, A.; Rostami, R.; Farzadkia, M. O<sub>3</sub>, O<sub>3</sub>/UV and O<sub>3</sub>/UV/ZnO for abatement of parabens in aqueous solutions: Effect of operational parameters and mineralization/biodegradability improvement. *Process Saf. Environ. Prot.* **2019**, *125*, 238–250. [[CrossRef](#)]
4. Zhou, R.; Liu, S.; He, F.R.; Ren, H.J.; Han, Z.H. Alkylpolyglycoside modified MnFe<sub>2</sub>O<sub>4</sub> with abundant oxygen vacancies boosting singlet oxygen dominated peroxy monosulfate activation for organic pollutants degradation. *Chemosphere* **2021**, *285*, 11. [[CrossRef](#)]
5. Pera-Titus, M.; García-Molina, V.; Baños, M.A.; Giménez, J.; Esplugas, S. Degradation of chlorophenols by means of advanced oxidation processes: A general review. *Appl. Catal. B* **2004**, *47*, 219–256. [[CrossRef](#)]
6. Jiang, G.; Zhu, B.; Sun, J.; Liu, F.; Wang, Y.; Zhao, C. Enhanced activity of ZnS (111) by N/Cu co-doping: Accelerated degradation of organic pollutants under visible light. *J. Environ. Sci.* **2023**, *125*, 244–257. [[CrossRef](#)]
7. Oh, S.-Y.; Kim, H.-W.; Park, J.-M.; Park, H.-S.; Yoon, C. Oxidation of polyvinyl alcohol by persulfate activated with heat, Fe<sup>2+</sup>, and zero-valent iron. *J. Hazard. Mater.* **2009**, *168*, 346–351. [[CrossRef](#)] [[PubMed](#)]
8. Liu, H.; Bruton, T.A.; Doyle, F.M.; Sedlak, D.L. In Situ Chemical Oxidation of Contaminated Groundwater by Persulfate: Decomposition by Fe(III)- and Mn(IV)-Containing Oxides and Aquifer Materials. *Environ. Sci. Technol.* **2014**, *48*, 10330–10336. [[CrossRef](#)] [[PubMed](#)]
9. Oyekunle, D.T.; Cai, J.; Gendy, E.A.; Chen, Z. Impact of chloride ions on activated persulfates based advanced oxidation process (AOPs): A mini review. *Chemosphere* **2021**, *280*, 130949. [[CrossRef](#)] [[PubMed](#)]
10. Liu, T.; Yao, B.; Luo, Z.; Li, W.; Li, C.; Ye, Z.; Gong, X.; Yang, J.; Zhou, Y. Applications and influencing factors of the biochar-persulfate based advanced oxidation processes for the remediation of groundwater and soil contaminated with organic compounds. *Sci. Total Environ.* **2022**, *836*, 155421. [[CrossRef](#)] [[PubMed](#)]
11. Huang, W.; Xiao, S.; Zhong, H.; Yan, M.; Yang, X. Activation of persulfates by carbonaceous materials: A review. *Chem. Eng. J.* **2021**, *418*, 129297. [[CrossRef](#)]
12. Oyekunle, D.T.; Gendy, E.A.; Ifthikar, J.; Chen, Z. Heterogeneous activation of persulfate by metal and non-metal catalyst for the degradation of sulfamethoxazole: A review. *Chem. Eng. J.* **2022**, *437*, 135277. [[CrossRef](#)]

13. Saputra, E.; Muhammad, S.; Sun, H.; Ang, H.-M.; Tade, M.O.; Wang, S. A comparative study of spinel structured  $\text{Mn}_3\text{O}_4$ ,  $\text{Co}_3\text{O}_4$  and  $\text{Fe}_3\text{O}_4$  nanoparticles in catalytic oxidation of phenolic contaminants in aqueous solutions. *J. Colloid Interface Sci.* **2013**, *407*, 467–473. [[CrossRef](#)] [[PubMed](#)]
14. Jabbar, T.A.; Ammar, S.H. Core/shell phosphomolybdic acid-supported magnetic silica nanocomposite (Ni@SiO<sub>2</sub>-PMo): Synthesis, characterization and its application as a recyclable antibacterial agent. *Colloid Interface Sci. Commun.* **2019**, *33*, 100214. [[CrossRef](#)]
15. Xu, L.; Wang, J. Fenton-like degradation of 2, 4-dichlorophenol using  $\text{Fe}_3\text{O}_4$  magnetic nanoparticles. *Appl. Catal. B* **2012**, *123*, 117–126. [[CrossRef](#)]
16. Ren, H.; Su, Y.; Han, X.; Zhou, R. Synthesis and characterization of saponin-modified  $\text{Fe}_3\text{O}_4$  nanoparticles as heterogeneous Fenton-catalyst with enhanced degradation of p-nitrophenol. *J. Chem. Technol. Biotechnol.* **2016**, *92*, 1421–1427. [[CrossRef](#)]
17. Zhou, R.; Lu, S.; Su, Y.; Li, T.; Ma, T.; Ren, H. Hierarchically fusiform CuO microstructures decorated with  $\text{Fe}_3\text{O}_4$  nanoparticles as novel persulfate activators for 4-aminobenzenesulfonic acid degradation in aqueous solutions. *J. Alloys Compd.* **2020**, *815*, 152394. [[CrossRef](#)]
18. Fang, G.-D.; Dionysiou, D.D.; Al-Abed, S.R.; Zhou, D.-M. Superoxide radical driving the activation of persulfate by magnetite nanoparticles: Implications for the degradation of PCBs. *Appl. Catal. B* **2013**, *129*, 325–332. [[CrossRef](#)]
19. Li, R.; Jin, X.; Megharaj, M.; Naidu, R.; Chen, Z. Heterogeneous Fenton oxidation of 2,4-dichlorophenol using iron-based nanoparticles and persulfate system. *Chem. Eng. J.* **2015**, *264*, 587–594. [[CrossRef](#)]
20. Jia, J.; Zhang, P.; Chen, L. The effect of morphology of  $\alpha\text{-MnO}_2$  on catalytic decomposition of gaseous ozone. *Catal. Sci. Technol.* **2016**, *6*, 5841–5847. [[CrossRef](#)]
21. Xu, L.; Xu, C.; Zhao, M.; Qiu, Y.; Sheng, G.D. Oxidative removal of aqueous steroid estrogens by manganese oxides. *Water Res.* **2008**, *42*, 5038–5044. [[CrossRef](#)]
22. Saputra, E.; Muhammad, S.; Sun, H.; Ang, H.M.; Tade, M.; Wang, S. Different crystallographic one-dimensional  $\text{MnO}_2$  nanomaterials and their superior performance in catalytic phenol degradation. *Environ. Sci. Technol.* **2013**, *47*, 5882–5887. [[CrossRef](#)] [[PubMed](#)]
23. Das, T.; Ganguly, S.; Remanan, S.; Ghosh, S.; Das, N. Mussel-inspired Ag/poly(norepinephrine)/ $\text{MnO}_2$  heterogeneous nanocatalyst for efficient reduction of 4-nitrophenol and 4-nitroaniline: An alternative approach. *Res. Chem. Intermed.* **2020**, *46*, 3629–3650. [[CrossRef](#)]
24. Zhao, H.; Cui, H.-J.; Fu, M.-L. Synthesis of core-shell structured  $\text{Fe}_3\text{O}_4@ \alpha\text{-MnO}_2$  microspheres for efficient catalytic degradation of ciprofloxacin. *RSC Adv.* **2014**, *4*, 39472–39475. [[CrossRef](#)]
25. Wang, Y.; Ren, H.; Pan, H.; Liu, J.; Zhang, L. Enhanced tolerance and remediation to mixed contaminants of PCBs and 2, 4-DCP by transgenic alfalfa plants expressing the 2, 3-dihydroxybiphenyl-1, 2-dioxygenase. *J. Hazard. Mater.* **2015**, *286*, 269–275. [[CrossRef](#)] [[PubMed](#)]
26. Saputra, E.; Muhammad, S.; Sun, H.; Patel, A.; Shukla, P.; Zhu, Z.; Wang, S.  $\alpha\text{-MnO}_2$  activation of peroxymonosulfate for catalytic phenol degradation in aqueous solutions. *Catal. Commun.* **2012**, *26*, 144–148. [[CrossRef](#)]
27. Jiang, Z.; Li, J.; Jiang, D.; Gao, Y.; Chen, Y.; Wang, W.; Cao, B.; Tao, Y.; Wang, L.; Zhang, Y. Removal of atrazine by biochar-supported zero-valent iron catalyzed persulfate oxidation: Reactivity, radical production and transformation pathway. *Environ. Res.* **2020**, *184*, 109260. [[CrossRef](#)]
28. Wu, H.; Wang, J.; Liu, H.; Fan, X. Performance, reaction pathway and kinetics of the enhanced dechlorination degradation of 2,4-dichlorophenol by Fe/Ni nanoparticles supported on attapulgite disaggregated by a ball milling-freezing process. *Materials* **2022**, *15*, 3957. [[CrossRef](#)]
29. Zhao, Y.; Zhao, Y.; Zhou, R.; Mao, Y.; Tang, W.; Ren, H. Insights into the degradation of 2,4-dichlorophenol in aqueous solution by alpha- $\text{MnO}_2$  nanowire activated persulfate: Catalytic performance and kinetic modeling. *RSC Adv.* **2016**, *6*, 35441–35448. [[CrossRef](#)]
30. Yan, J.; Lei, M.; Zhu, L.; Anjum, M.N.; Zou, J.; Tang, H. Degradation of sulfamonomethoxine with  $\text{Fe}_3\text{O}_4$  magnetic nanoparticles as heterogeneous activator of persulfate. *J. Hazard. Mater.* **2011**, *186*, 1398–1404. [[CrossRef](#)]
31. Xia, C.; Liu, Q.; Zhao, L.; Wang, L.; Tang, J. Enhanced degradation of petroleum hydrocarbons in soil by FeS@BC activated persulfate and its mechanism. *Sep. Purif. Technol.* **2022**, *282*, 120060. [[CrossRef](#)]
32. Yuan, Y.; Tao, H.; Fan, J.; Ma, L. Degradation of p-chloroaniline by persulfate activated with ferrous sulfide ore particles. *Chem. Eng. J.* **2015**, *268*, 38–46. [[CrossRef](#)]
33. Couttenye, R.; Huang, K.-C.; Hoag, G.; Suib, S. Evidence of Sulfate Free Radical ( $\text{SO}_4^{\cdot -}$ ) Formation under Heat-Assisted Persulfate Oxidation of MTBE. *Bull. Educ. Res. Pract.* **2003**, *8*, 345–350.
34. Do, S.-H.; Kwon, Y.-J.; Kong, S.-H. Effect of metal oxides on the reactivity of persulfate/Fe(II) in the remediation of diesel-contaminated soil and sand. *J. Hazard. Mater.* **2010**, *182*, 933–936. [[CrossRef](#)]
35. Hou, L.; Zhang, H.; Xue, X. Ultrasound enhanced heterogeneous activation of peroxydisulfate by magnetite catalyst for the degradation of tetracycline in water. *Sep. Purif. Technol.* **2012**, *84*, 147–152. [[CrossRef](#)]
36. Xin Zhang, Y.; Long Guo, X.; Huang, M.; Dong Hao, X.; Yuan, Y.; Hua, C. Engineering birnessite-type  $\text{MnO}_2$  nanosheets on fiberglass for pH-dependent degradation of methylene blue. *J. Phys. Chem. Solids* **2015**, *83*, 40–46. [[CrossRef](#)]
37. Liu, J.; Zhao, Z.; Shao, P.; Cui, F. Activation of peroxymonosulfate with magnetic  $\text{Fe}_3\text{O}_4\text{-}\alpha\text{-MnO}_2$  core-shell nanocomposites for 4-chlorophenol degradation. *Chem. Eng. J.* **2015**, *262*, 854–861. [[CrossRef](#)]

38. Prélot, B.; Poinignon, C.; Thomas, F.; Schouller, E.; Villiéras, F. Structural–chemical disorder of manganese dioxides: 1. Influence on surface properties at the solid–electrolyte interface. *J. Colloid Interface Sci.* **2003**, *257*, 77–84. [[CrossRef](#)]
39. Rahmani, A.; Salari, M.; Tari, K.; Shabanloo, A.; Shabanloo, N.; Bajalan, S. Enhanced degradation of furfural by heat-activated persulfate/nZVI-rGO oxidation system: Degradation pathway and improving the biodegradability of oil refinery wastewater. *J. Environ. Chem. Eng.* **2020**, *8*, 104468. [[CrossRef](#)]
40. Liang, H.; Sun, H.; Patel, A.; Shukla, P.; Zhu, Z.H.; Wang, S. Excellent performance of mesoporous Co<sub>3</sub>O<sub>4</sub>/MnO<sub>2</sub> nanoparticles in heterogeneous activation of peroxymonosulfate for phenol degradation in aqueous solutions. *Appl. Catal. B* **2012**, *127*, 330–335. [[CrossRef](#)]
41. Gan, P.; Zhang, Z.; Hu, Y.; Li, Y.; Ye, J.; Tong, M.; Liang, J. Insight into the role of Fe in the synergetic effect of persulfate/sulfite and Fe<sub>2</sub>O<sub>3</sub>@g-C<sub>3</sub>N<sub>4</sub> for carbamazepine degradation. *Sci. Total Environ.* **2022**, *819*, 152787. [[CrossRef](#)] [[PubMed](#)]